Biomedical Optics EXPRESS

Heartbeat OCT: *in vivo* intravascular megahertz-optical coherence tomography

Tianshi Wang,[1,6,*] Tom Pfeiffer,[2,3,6] Evelyn Regar,[1] Wolfgang Wieser,[2] Heleen van Beusekom,[1] Charles T. Lancee,[1] Geert Springeling,[1] Ilona Krabbendam,[1] Antonius F.W. van der Steen,[1,4,5] Robert Huber,[2,3] and Gijs van Soest[1]

[1]*Thorax Center, Erasmus University Medical Center, P. O. Box 2040, Rotterdam 3000 CA, The Netherlands*
[2]*Lehrstuhl für Biomolekulare Optik, Fakultät für Physik, Ludwig-Maximilians-Universität München, Oettingenstr. 67, München 80538, Germany*
[3]*Institut für Biomedizinische Optik, Universität zu Lübeck, Peter-Monnik-Weg 4, 23562 Lübeck Germany*
[4]*Shenzhen Institutes of Advanced Technology, Chinese Academy of Sciences, 518055 Shenzhen, China*
[5]*Department of Imaging science and Technology, Delft University of Technology, Postbus 5, Delft 2600 AA, The Netherlands*
[6]*These authors contributed equally to this work*
**tswang1983@gmail.com*

Abstract: Cardiac motion artifacts, non-uniform rotational distortion and undersampling affect the image quality and the diagnostic impact of intravascular optical coherence tomography (IV-OCT). In this study we demonstrate how these limitations of IV-OCT can be addressed by using an imaging system that we called "Heartbeat OCT", combining a fast Fourier Domain Mode Locked laser, fast pullback, and a micromotor actuated catheter, designed to examine a coronary vessel in less than one cardiac cycle. We acquired *in vivo* data sets of two coronary arteries in a porcine heart with both Heartbeat OCT, working at 2.88 MHz A-line rate, 4000 frames/s and 100 mm/s pullback speed, and with a commercial system. The *in vivo* results show that Heartbeat OCT provides faithfully rendered, motion-artifact free, fully sampled vessel wall architecture, unlike the conventional IV-OCT data. We present the Heartbeat OCT system in full technical detail and discuss the steps needed for clinical translation of the technology.

OCIS codes: (170.4500) Optical coherence tomography; (170.3880) Medical and biological imaging; (170.2150) Endoscopic imaging; (110.6880) Three-dimensional image acquisition; (110.2350) Fiber optics imaging; (120.5800) Scanners; (120.3890) Medical optics instrumentation.

References and links

1. D. Huang, E. A. Swanson, C. P. Lin, J. S. Schuman, W. G. Stinson, W. Chang, M. R. Hee, T. Flotte, K. Gregory, C. A. Puliafito, and et, "Optical coherence tomography," Science **254**(5035), 1178–1181 (1991).
2. G. J. Tearney, S. A. Boppart, B. E. Bouma, M. E. Brezinski, N. J. Weissman, J. F. Southern, and J. G. Fujimoto, "Scanning single-mode fiber optic catheter-endoscope for optical coherence tomography," Opt. Lett. **21**(7), 543–545 (1996).
3. G. J. Tearney, E. Regar, T. Akasaka, T. Adriaenssens, P. Barlis, H. G. Bezerra, B. Bouma, N. Bruining, J. M. Cho, S. Chowdhary, M. A. Costa, R. de Silva, J. Dijkstra, C. Di Mario, D. Dudek, E. Falk, M. D. Feldman, P. Fitzgerald, H. M. Garcia-Garcia, N. Gonzalo, J. F. Granada, G. Guagliumi, N. R. Holm, Y. Honda, F. Ikeno, M. Kawasaki, J. Kochman, L. Koltowski, T. Kubo, T. Kume, H. Kyono, C. C. Lam, G. Lamouche, D. P. Lee, M. B. Leon, A. Maehara, O. Manfrini, G. S. Mintz, K. Mizuno, M. A. Morel, S. Nadkarni, H. Okura, H. Otake, A. Pietrasik, F. Prati, L. Räber, M. D. Radu, J. Rieber, M. Riga, A. Rollins, M. Rosenberg, V. Sirbu, P. W. Serruys, K. Shimada, T. Shinke, J. Shite, E. Siegel, S. Sonoda, M. Suter, S. Takarada, A. Tanaka, M. Terashima, T. Thim, S. Uemura, G. J. Ughi, H. M. van Beusekom, A. F. van der Steen, G. A. van Es, G. van Soest, R. Virmani, S. Waxman, N. J. Weissman, and G. Weisz; International Working Group for Intravascular Optical Coherence Tomography (IWG-IVOCT), "Consensus standards for acquisition, measurement, and reporting of intravascular optical coherence tomography studies: a report from the International Working Group for Intravascular Optical Coherence Tomography Standardization and Validation," J. Am. Coll. Cardiol. **59**(12), 1058–1072 (2012).

#250211 Received 15 Sep 2015; revised 26 Oct 2015; accepted 30 Oct 2015; published 23 Nov 2015

4. S. H. Yun, G. J. Tearney, B. J. Vakoc, M. Shishkov, W. Y. Oh, A. E. Desjardins, M. J. Suter, R. C. Chan, J. A. Evans, I.-K. Jang, N. S. Nishioka, J. F. de Boer, and B. E. Bouma, "Comprehensive volumetric optical microscopy in vivo," Nat. Med. **12**(12), 1429–1433 (2007).
5. I. K. Jang, G. Tearney, and B. Bouma, "Visualization of tissue prolapse between coronary stent struts by optical coherence tomography: comparison with intravascular ultrasound," Circulation **104**(22), 2754 (2001).
6. F. Prati, L. Di Vito, G. Biondi-Zoccai, M. Occhipinti, A. La Manna, C. Tamburino, F. Burzotta, C. Trani, I. Porto, V. Ramazzotti, F. Imola, A. Manzoli, L. Materia, A. Cremonesi, and M. Albertucci, "Angiography alone versus angiography plus optical coherence tomography to guide decision-making during percutaneous coronary intervention: the Centro per la Lotta contro l'Infarto-Optimisation of Percutaneous Coronary Intervention (CLI-OPCI) study," EuroIntervention **8**(7), 823–829 (2012).
7. N. Meneveau, F. Ecarnot, G. Souteyrand, P. Motreff, C. Caussin, E. Van Belle, P. Ohlmann, O. Morel, A. Grentzinger, M. Angioi, R. Chopard, and F. Schiele, "Does optical coherence tomography optimize results of stenting? Rationale and study design," Am. Heart J. **168**(2), 175–181 (2014).
8. Y. Kawase, Y. Suzuki, F. Ikeno, R. Yoneyama, K. Hoshino, H. Q. Ly, G. T. Lau, M. Hayase, A. C. Yeung, R. J. Hajjar, and I. K. Jang, "Comparison of nonuniform rotational distortion between mechanical IVUS and OCT using a phantom model," Ultrasound Med. Biol. **33**(1), 67–73 (2007).
9. W. Kang, H. Wang, Z. Wang, M. W. Jenkins, G. A. Isenberg, A. Chak, and A. M. Rollins, "Motion artifacts associated with in vivo endoscopic OCT images of the esophagus," Opt. Express **19**(21), 20722–20735 (2011).
10. T. Okamura, Y. Onuma, H. M. Garcia-Garcia, N. Bruining, and P. W. Serruys, "High-speed intracoronary optical frequency domain imaging: implications for three-dimensional reconstruction and quantitative analysis," EuroIntervention **7**(10), 1216–1226 (2012).
11. V. Farooq, B. D. Gogas, T. Okamura, J. H. Heo, M. Magro, J. Gomez-Lara, Y. Onuma, M. D. Radu, S. Brugaletta, G. van Bochove, R. J. van Geuns, H. M. Garcìa-Garcìa, and P. W. Serruys, "Three-dimensional optical frequency domain imaging in conventional percutaneous coronary intervention: the potential for clinical application," Eur. Heart J. **34**(12), 875–885 (2013).
12. N. S. van Ditzhuijzen, A. Karanasos, N. Bruining, M. van den Heuvel, O. Sorop, J. Ligthart, K. Witberg, H. M. Garcia-Garcia, F. Zijlstra, D. J. Duncker, H. M. van Beusekom, and E. Regar, "The impact of Fourier-Domain optical coherence tomography catheter induced motion artefacts on quantitative measurements of a PLLA-based bioresorbable scaffold," Int. J. Cardiovasc. Imaging **30**(6), 1013–1026 (2014).
13. T. Okamura, Y. Onuma, H. M. Garcia-Garcia, R. J. van Geuns, J. J. Wykrzykowska, C. Schultz, W. J. van der Giessen, J. Ligthart, E. Regar, and P. W. Serruys, "First-in-man evaluation of intravascular optical frequency domain imaging (OFDI) of Terumo: a comparison with intravascular ultrasound and quantitative coronary angiography," EuroIntervention **6**(9), 1037–1045 (2011).
14. H. S. Cho, S. J. Jang, K. Kim, A. V. Dan-Chin-Yu, M. Shishkov, B. E. Bouma, and W. Y. Oh, "High frame-rate intravascular optical frequency-domain imaging in vivo," Biomed. Opt. Express **5**(1), 223–232 (2014).
15. L. N. Andreasen, I. R. Balleby, and N. R. Holm, "Uncertain detection of nonuniform scaffold expansion patterns using optical coherence tomography," JACC Cardiovasc. Interv. **8**(8), 1135–1136 (2015).
16. N. Kollias, M. L. Dufour, C.-E. Bisaillon, G. Lamouche, S. Vergnole, M. Hewko, F. D'Amours, C. Padioleau, and M. Sowa, "Tools for experimental characterization of the non-uniform rotational distortion in intravascular OCT probes," in *Proc. SPIE*, 2011), 788339.
17. T. Wang, W. Wieser, G. Springeling, R. Beurskens, C. T. Lancee, T. Pfeiffer, A. F. van der Steen, R. Huber, and G. van Soest, "Intravascular optical coherence tomography imaging at 3200 frames per second," Opt. Lett. **38**(10), 1715–1717 (2013).
18. O. O. Ahsen, H. C. Lee, M. G. Giacomelli, Z. Wang, K. Liang, T. H. Tsai, B. Potsaid, H. Mashimo, and J. G. Fujimoto, "Correction of rotational distortion for catheter-based en face OCT and OCT angiography," Opt. Lett. **39**(20), 5973–5976 (2014).
19. R. Huber, M. Wojtkowski, and J. G. Fujimoto, "Fourier Domain Mode Locking (FDML): A new laser operating regime and applications for optical coherence tomography," Opt. Express **14**(8), 3225–3237 (2006).
20. T. Wang, G. van Soest, and A. F. W. van der Steen, "A micromotor catheter for intravascular optical coherence tomography," Engineering **1**, 15–17 (2015).
21. T. Wang, T. Pfeiffer, E. Regar, W. Wieser, H. M. M. van Beusekom, C. T. Lancee, G. Springeling, I. Krabbendam, A. F. W. van der Steen, R. Huber, and G. van Soest, "Heartbeat optical coherence tomography: motion-free three-dimensional in vivo coronary artery microscopy," J. Am. Coll. Cardiol. Img. in press.
22. T. Wang, C. Lancée, R. Beurskens, J. Meijer, B. Knapen, A. F. W. van der Steen, and G. van Soest, "Development of a high-speed synchronous micro motor and its application in intravascular imaging," Sens. Act. A **218**, 60–68 (2014).
23. D. C. Adler, Y. Chen, R. Huber, J. Schmitt, J. Connolly, and J. G. Fujimoto, "Three-dimensional endomicroscopy using optical coherence tomography," Nat. Photonics **1**(12), 709–716 (2007).
24. W. Wieser, B. R. Biedermann, T. Klein, C. M. Eigenwillig, and R. Huber, "Multi-megahertz OCT: High quality 3D imaging at 20 million A-scans and 4.5 GVoxels per second," Opt. Express **18**(14), 14685–14704 (2010).
25. W. Wieser, T. Klein, D. C. Adler, F. Trépanier, C. M. Eigenwillig, S. Karpf, J. M. Schmitt, and R. Huber, "Extended coherence length megahertz FDML and its application for anterior segment imaging," Biomed. Opt. Express **3**(10), 2647–2657 (2012).
26. R. Huber, D. C. Adler, and J. G. Fujimoto, "Buffered Fourier domain mode locking: Unidirectional swept laser sources for optical coherence tomography imaging at 370,000 lines/s," Opt. Lett. **31**(20), 2975–2977 (2006).

#250211 Received 15 Sep 2015; revised 26 Oct 2015; accepted 30 Oct 2015; published 23 Nov 2015

27. G. van Soest, J. G. Bosch, and A. F. van der Steen, "Azimuthal registration of image sequences affected by nonuniform rotation distortion," IEEE Trans. Inf. Technol. Biomed. **12**(3), 348–355 (2008).
28. C. Gatta, O. Pujol, O. Rodriguez Leor, J. Mauri Ferre, and P. Radeva, "Fast rigid registration of vascular structures in IVUS sequences," IEEE Trans. Inf. Technol. Biomed. **13**(6), 1006–1011 (2009).
29. G. J. Ughi, T. Adriaenssens, M. Larsson, C. Dubois, P. R. Sinnaeve, M. Coosemans, W. Desmet, and J. D'hooge, "Automatic three-dimensional registration of intravascular optical coherence tomography images," J. Biomed. Opt. **17**(2), 026005 (2012).
30. C. Sun, F. Nolte, K. H. Cheng, B. Vuong, K. K. Lee, B. A. Standish, B. Courtney, T. R. Marotta, A. Mariampillai, and V. X. Yang, "In vivo feasibility of endovascular Doppler optical coherence tomography," Biomed. Opt. Express **3**(10), 2600–2610 (2012).
31. J. Li, M. de Groot, F. Helderman, J. Mo, J. M. Daniels, K. Grünberg, T. G. Sutedja, and J. F. de Boer, "High speed miniature motorized endoscopic probe for optical frequency domain imaging," Opt. Express **20**(22), 24132–24138 (2012).
32. T. H. Tsai, B. Potsaid, Y. K. Tao, V. Jayaraman, J. Jiang, P. J. Heim, M. F. Kraus, C. Zhou, J. Hornegger, H. Mashimo, A. E. Cable, and J. G. Fujimoto, "Ultrahigh speed endoscopic optical coherence tomography using micromotor imaging catheter and VCSEL technology," Biomed. Opt. Express **4**(7), 1119–1132 (2013).
33. St. Jude Medical, "ILUMIEN™ OPTIS™ PCI Optimization™ System" (2013), retrieved Sept. 9, 2015, https://professional-intl.sjm.com/resources/vascular/intravascular-diagnostics-and-imaging/intravascular-diagnostics-and-imaging-system-ffr-oct/ilumien-optis-pci-optimization-system.
34. H. Yoo, J. W. Kim, M. Shishkov, E. Namati, T. Morse, R. Shubochkin, J. R. McCarthy, V. Ntziachristos, B. E. Bouma, F. A. Jaffer, and G. J. Tearney, "Intra-arterial catheter for simultaneous microstructural and molecular imaging in vivo," Nat. Med. **17**(12), 1680–1684 (2011).
35. M. Villiger, E. Z. Zhang, S. K. Nadkarni, W.-Y. Oh, B. J. Vakoc, and B. E. Bouma, "Spectral binning for mitigation of polarization mode dispersion artifacts in catheter-based optical frequency domain imaging," Opt. Express **21**(14), 16353–16369 (2013).
36. X. Li, T. H. Ko, and J. G. Fujimoto, "Intraluminal fiber-optic Doppler imaging catheter for structural and functional optical coherence tomography," Opt. Lett. **26**(23), 1906–1908 (2001).
37. G. van Soest, T. Goderie, E. Regar, S. Koljenović, G. L. van Leenders, N. Gonzalo, S. van Noorden, T. Okamura, B. E. Bouma, G. J. Tearney, J. W. Oosterhuis, P. W. Serruys, and A. F. van der Steen, "Atherosclerotic tissue characterization in vivo by optical coherence tomography attenuation imaging," J. Biomed. Opt. **15**(1), 011105 (2010).
38. B. F. Kennedy, K. M. Kennedy, and D. D. Sampson, "A review of optical coherence elastography: fundamentals, techniques and prospects," IEEE J. Sel. Top. Quantum Electron. **20**(2), 7101217 (2014).

1. Introduction

Intravascular Optical Coherence Tomography (IV-OCT) [1–4] is a catheter-based imaging technique that provides comprehensive volumetric microscopy of the artery, with 10-15 μm resolution. IV-OCT has been available for clinical use for about a decade [5], and has generated a wealth of data that has deepened our understanding of coronary artery disease and catheter-based interventions on the vasculature [6, 7]. A number of issues, however – cardiac motion artifacts, undersampling and non-uniform rotational distortion (NURD) chiefly among them – affect the quality and interpretability of IV-OCT images [8–12]. The optical coherence tomography (OCT) imaging speed is limited by the scanning speed of the catheter and the speed of the OCT engine. Commercial systems acquire 3D data sets in 3-5 s, with a pullback speed of 20-40 mm/s and a frame rate of 100-180 frames/s [11, 13, 14]. The duration of the acquisition covers several cardiac cycles, which leads to image artifacts as a result of catheter motion during pullback. Longitudinal displacement of the vessel relative to the catheter causes inaccuracy in frame spacing, and possibly frame order, affecting length measurements and the fidelity of the longitudinal rendering and 3D reconstruction of the data [10–12, 15]. The frame spacing in commercial pullbacks is typically 200 μm, while the beam width is around 30 μm, which means that the rendered volume is undersampled by a factor of 7 in the longitudinal direction. Consequently, there is a distinct difference in image quality of the longitudinal rendering compared to the cross-sectional images [10, 11]. NURD is a result of rotational friction of the hollow drive-shaft in the catheter, leading to variable torque transfer from the proximal motor to the catheter tip [8, 9, 16]. It appears as distortion in a single frame, or as wobbling of frames relative to each other.

The motion and sampling limitations of IV-OCT can be overcome by acquiring all data in between two subsequent left-ventricle contractions, avoiding excessive motion. Given a

#250211 Received 15 Sep 2015; revised 26 Oct 2015; accepted 30 Oct 2015; published 23 Nov 2015

typical heart rate between 60 and 70 per minute for patients undergoing cardiac catheterization, and accounting for variability in motion patterns at different locations of the heart, 5-7 cm of coronary artery can be scanned at a pullback speed of 100 mm/s. Full sampling of the data in the longitudinal direction requires that the frame spacing is smaller than the width of the imaging beam (typically 30 μm for IV-OCT catheters), meaning we target a frame rate of > 3 kHz. Synchronization with the cardiac cycle can be achieved by deriving a trigger signal from the electrocardiogram (ECG) with an appropriate delay. We call this concept "*Heartbeat OCT*".

Fast and uniform scanning can be achieved with a distal actuator [8, 9, 16–18]. Based on this principle, we reported an IV-OCT system imaging at 3200 frames/s [17]. Using a faster Fourier Domain Mode Locked (FDML) laser [19] and a refined micro-motor-based catheter, we developed a system that achieves an imaging speed up to 5600 frames/s which could be demonstrated *in vitro* [20]. It was deployed in a first *in vivo* experiment at 4000 frames/s [21]. In this study, we characterize the Heartbeat OCT system in full technical detail and present a comparison between Heartbeat OCT a conventional IV-OCT scanner *in vivo*. We conducted imaging experiments with both systems in a porcine model of percutaneous coronary intervention (PCI), both in a native coronary artery and in an instrumented artery that sustained vessel injury during the intervention. The images acquired are compared in various visualizations to comprehensively demonstrate the value of Heartbeat OCT.

2. Methods

2.1 Synchronous micromotor-based catheter

For this study, we developed a micro-motor-based intravascular catheter as shown in Fig. 1(a). The micro motor is a two-phase, four-pole synchronous motor consisting of a permanent magnet rotor and a single-strand coil [22]. The dimensions of the motor are 2.0 mm length and 1.0 mm outer diameter (OD). Four copper leads were soldered to the motor to provide the driving current. The current signal was programmed using an arbitrary waveform generator (Agilent, 33522A, USA) and applied to the motor through a balanced current amplifier.

A 0.3 mm mirror (Edmund Optics, USA) was attached on the shaft by a plastic holder. A fiber probe with a gradient refractive index (GRIN) lens (Agiltron, USA) at the tip was used to transmit and focus the laser beam. The laser beam forms a beam waist of 29 μm at 1.1 mm distance from the tube. The beam diameter on the mirror was 112 μm, around 1/3 of the mirror size, rendering the optical alignment robust against catheter bending; motion of the shaft of the motor is minimal because of its tight mechanical tolerance (< 10 μm). The combined length of the motor and GRIN lens mount was 5.3 mm. The fiber probe and the motor were mounted into a 1.2 mm OD biocompatible polyether block amide (Pebax, Arkema, France) tube without welds or joints for mechanical stability. The proximal end of the catheter is terminated by a stainless steel tube that can be clamped on the pullback motor, also providing optical and electrical connectors. The photo and schematic of the catheter tip is shown in Fig. 1(a). The micro motor is radio-opaque and can be used to track the position of the catheter tip as shown in Fig. 1(b) and Visualization 1. The final dimension of the catheter is 1.2 mm OD and 1.7 m length.

#250211 Received 15 Sep 2015; revised 26 Oct 2015; accepted 30 Oct 2015; published 23 Nov 2015

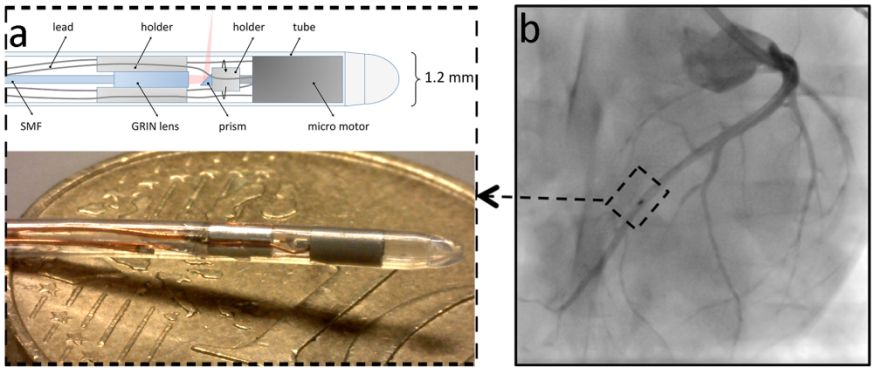

Fig. 1. (a) The intravascular catheter tip contains the focusing optics and a mirror mounted on the axis of a micro motor that drives the rotation of the mirror. The photo shows the catheter tip on a 10 Eurocent coin. (b) Angiography of the swine heart during *in vivo* imaging (see Visualization 1). The micro motor (dotted box in b) is radio-opaque and can be used to track the position of the catheter tip. SMF = single mode fiber; GRIN = gradient refractive index.

2.2 Electrocardiography triggered pullback and data acquisition

Data acquisition was synchronized with the cardiac cycle through an electrocardiography (ECG) triggered pullback system. The R-peak of the ECG signal was used to generate a trigger signal with a user-controlled delay, to start the data acquisition. The delay was set to avoid the strong cardiac motion during the T-wave caused by the movement of the left ventricle contraction [11]. There may be individual variability in the optimal delay setting, and it is likely specific for each location on the heart and will thus change per vessel. In the present experiment we set the delay heuristically by inspection of the angiogram. A linear motor (Aerotech, USA) was triggered from the same signal. The motor was programmed to pull back at 100 mm/s, with an acceleration of 30 m/s^2. Figure 2 shows the ECG triggered pullback and data acquisition.

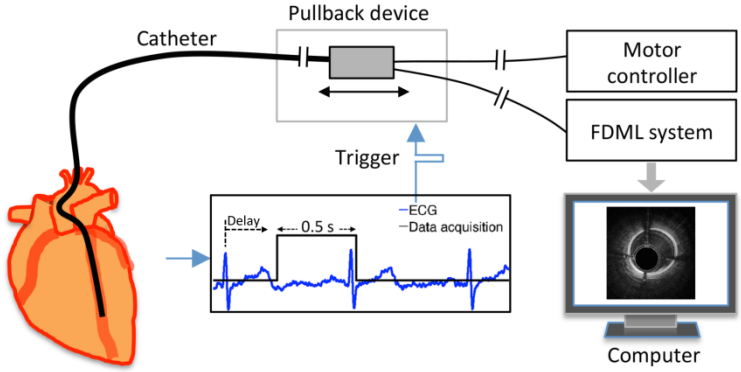

Fig. 2. Schematic of the electrocardiography (ECG) triggered pullback and data acquisition.

2.3 FDML laser-based OCT engine

The OCT engine was built based on an FDML laser with a center wavelength of 1310 nm and a sweep rate of 2.88 MHz as shown in Fig. 3(a) [19, 23, 24]. In the OCT engine, 90% of the laser power was sent to the sample while 10% of the laser power was sent to the reference mirror. A 1.6 GHz balanced photo receiver (Thorlabs, PDB480C-AC, USA) and a 4 GS/s 8 bit data acquisition board (Gage, COBRAMAX, USA) were used to record the interferogram.

The FDML laser uses a home built ultra-high speed tunable Fabry-Perot filter running at 360 kHz tuning frequency. A specially designed chirped fiber Bragg grating with a

#250211 Received 15 Sep 2015; revised 26 Oct 2015; accepted 30 Oct 2015; published 23 Nov 2015

transmission of around 40% is used for intra cavity dispersion compensation and as an output coupler [25]. The semiconductor optical amplifier (SOA) current is modulated to restrict the duty cycle of the laser to 12.5% as needed for buffering. During laser-on time the filter transmission is tuned 108 nm over a central wavelength of 1310 nm. An additional buffer stage [26] increases the fundamental sweep rate eightfold resulting in an effective A-line rate of 2.88 MHz. After passing an additional booster SOA the average output power is 70mW. Figure 3(b) shows the schematic of the FDML laser.

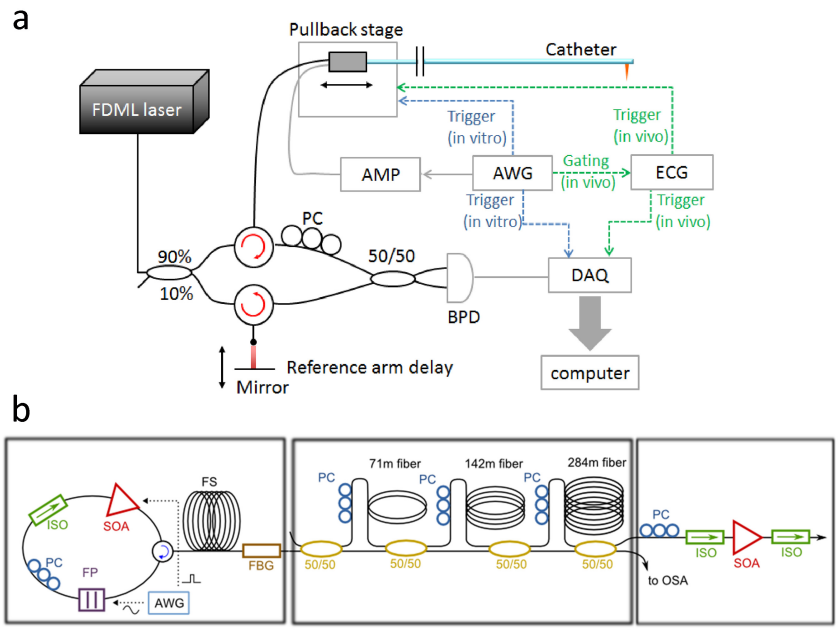

Fig. 3. (a) Schematic of the imaging system. Dotted green line: *in vivo* triggering. Dotted blue line: *in vitro* triggering. (b) Schematic of the FDML laser. AMP = amplifier; AWG = arbitrary waveform generator; PC = polarization controller; BPD = balanced photo diodes. DAQ = data acquisition. SOA = semiconductor optical amplifiers; OSA = optical spectrum analyzer; FBG = fiber Bragg grating; ISO = isolator; FP = Fabry-Perot filter. FS = fiber spool with monotonic dispersion.

2.4 Animal imaging procedure

The Heartbeat OCT catheter was inserted manually through the guiding catheter. The radio-opaque micro motor allows tracking of the catheter tip by fluoroscopy (Siemens, Artis Zee, Germany). After positioning the catheter tip distally into the coronary artery, the experimenter started the imaging procedure by accelerating the micro motor for 3 s and arming the data acquisition and pullback triggers. X-ray contrast dye (GE Healthcare, VISIPAQUE, USA) was used to flush the artery at a rate of 3-4 ml/s from an automated injector pump (Medrad, Mark V ProVis, USA). The cross-sectional images and longitudinal rendering were displayed on the screen immediately after pullback.

2.5 Image alignment and volume reconstruction

After applying a standard OCT signal processing chain - in short: background subtraction, resampling, FFT and magnitude computation - the resulting images had to be realigned to compensate the tiny rotation error of the motor (< 5°). This was automatically done by detecting the wire shadows and using them as fiducial markers [18]. We also observed a slightly change of the optical path length due to the heating of the fiber in the catheter during the data set acquisition. This was compensated by shifting the inner tube reflection to a depth

#250211 Received 15 Sep 2015; revised 26 Oct 2015; accepted 30 Oct 2015; published 23 Nov 2015

of 0.5 mm in every frame. Two opposite A-lines with 180° shift were then selected in each frame. From all frames, these selected A-lines created the longitudinal rendering. To construct a transverse cross-sectional video, A-lines were downsampled by a factor 2 to create an image of approximately 700 x 700 pixels. The 3D reconstruction (Osirix, Pixmeo, USA) was generated based on the transverse cross-sectional images in which the reflection of the catheter tube was removed in advance.

3. Results

3.1 System performance

The 108 nm sweep range of the FDML laser provided an axial × transverse resolution of 13 µm × 29 µm with an imaging depth of up to 4.0 mm (in air). With a power of 40 mW on the sample, the sensitivity of Heartbeat OCT was measured to be 98 dB, which is close to the shot noise limit of 102 dB. The current-driven motor can generate a temperature rise due to thermal dissipation of the resistive heating. With a driving current up to 0.7 A, the temperature rise was observed to be acceptable at < 1°C during a measurement cycle that consisted of 3 s spin up and 1 s for data acquisition. The maximum rotation speed at this current was 4000 rev/s enabling the acquisition of 4000 frames/s *in vivo*, with 2.88 million A-lines per second. With a driving current of 1.0 A, a maximum speed of 5600 rev/s was achieved, but not implemented *in vivo* because of heating by up to 4°C. The spectrum of the laser is shown in Fig. 4(a) and the sensitivity performance (roll-off) is shown in Fig. 4(b).

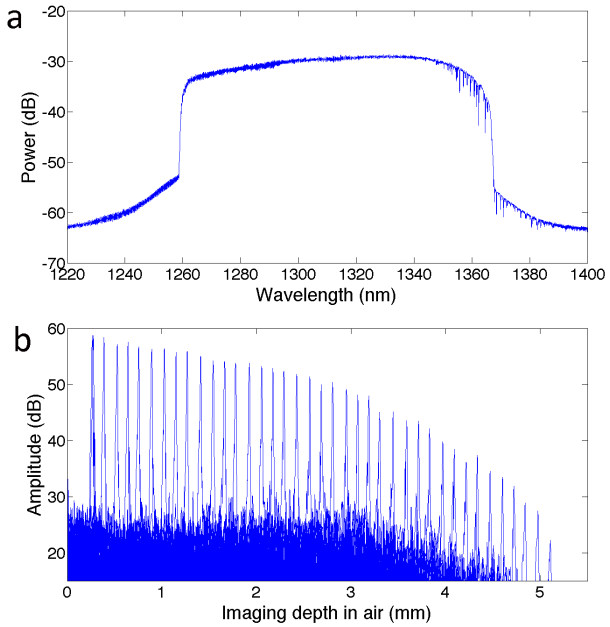

Fig. 4. (a) Spectrum of the FDML laser and (b) Roll-off performance of the system.

3.2 In vivo imaging of native coronary vasculature

In vivo imaging experiments were carried out in a healthy Yorkshire land swine (37 kg). Pullback recordings were acquired in the LAD coronary artery and the obtuse marginal (OM) branch of the left circumflex coronary artery. The R-wave of the ECG signal triggered the data acquisition and the pullback with 0.27s delay. In the LAD, approximately 50.0 mm artery was imaged within 0.5 s with an imaging speed of 4000 frames/s and a pullback speed of 100 mm/s. Figure 5(a), the cross-sectional image of the artery, clearly shows the layered

#250211 Received 15 Sep 2015; revised 26 Oct 2015; accepted 30 Oct 2015; published 23 Nov 2015

tissue of the artery wall such as internal elastic lamina, media and adventitia, which can also be identified on the co-located histology section as shown in Fig. 5(b). The entire cross-sectional pullback recording is also shown in Visualization 2. As the data set was acquired during a part of the cardiac cycle with minimal motion, the longitudinal rendering (Fig. 5(c)) shows a smooth lumen of the artery without discontinuities or variable vessel caliber. The 25 µm frame spacing results in a densely sampled, smooth longitudinal rendering. The layered structures of the artery wall are clearly visible in the longitudinal rendering (Fig. 5(d) and Visualization 3), in addition to the familiar appearance in the cross-sectional images. Figure 5(e) shows the 3D fly-through inside the artery lumen, and Fig. 5(f) shows the 3D reconstruction of the entire artery lumen cut along the vertical plane.

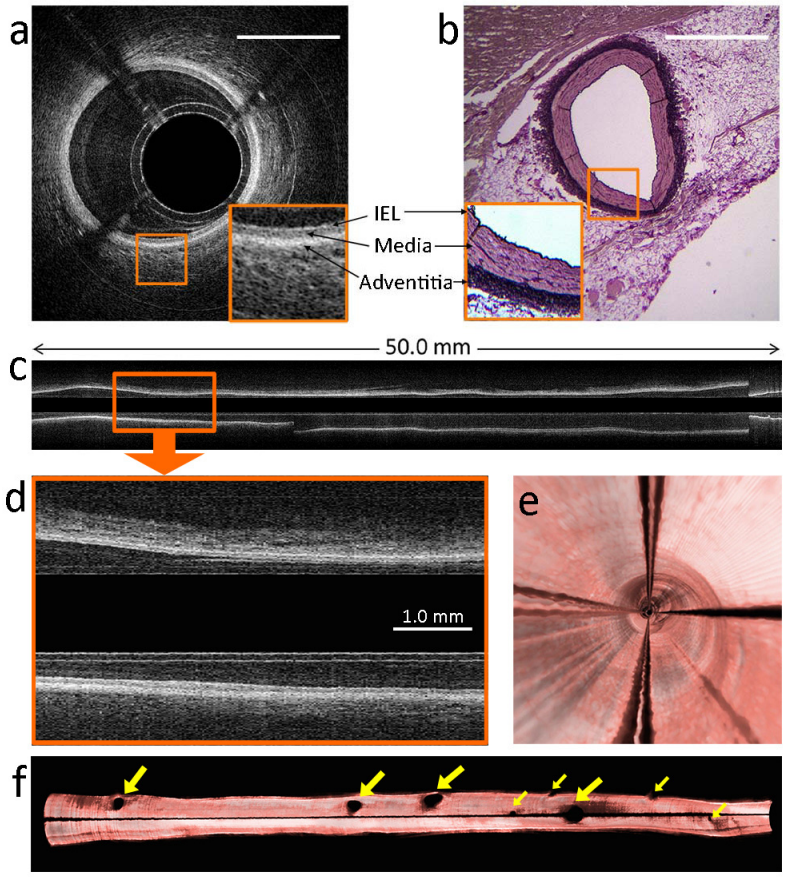

Fig. 5. *In vivo* images of swine LAD coronary artery. The images were acquired within one cardiac cycle using Heartbeat OCT. The imaging speed was 4000 frames/s, and the pullback speed was 100 mm/s. (a) Cross-sectional image of the healthy artery wall (see Visualization 2). The magnified part shows layered structures as internal elastic lamina (IEL), media and adventitia. Scale bar = 1.0 mm. (b) The same layers can be identified in a co-located histological section of the artery wall (resorcin fuchsine staining). (c) Longitudinal rendering of the entire artery (see Visualization 3). The magnification (d) shows a healthy artery wall with the layered structures. (e) 3D fly-through inside the artery lumen. (f) 3D re-construction of the artery cut along the vertical plane. The yellow arrows indicate septal branches. The shadow is caused by the motor lead.

In the OM branch, pullbacks were acquired using both Heartbeat OCT and a commercial IV-OCT system (C7XR with Dragonfly catheter, St. Jude Medical, St. Paul, Minnesota) sequentially. For Heartbeat OCT, the imaging speed was set to 3200 frames/s with a lower

#250211 Received 15 Sep 2015; revised 26 Oct 2015; accepted 30 Oct 2015; published 23 Nov 2015

driving current of 0.6 A for the motor, and the pullback speed was 100 mm/s. The commercial system was operating at 100 frames/s imaging speed and 20 mm/s pullback speed. Co-located cross-sectional images in the artery display the normal wall with similar feature definition in both systems (Fig. 6(a) and 6(d)). As a consequence of both NURD and cardiac motion, the pullback data from the commercial system has an irregular lumen (Fig. 6(b)); the insets show that frame-by-frame inspection of the data reveals repeated features in frame 13 and 25, although rotated by 60° (Fig. 6(b)). In the data of Heartbeat OCT, the cardiac motion artifacts and NURD are absent and the vessel is smooth and straight as expected for a healthy coronary artery (Fig. 6(e)). In the longitudinal rendering, the vessel wall is visualized in full detail by Heartbeat OCT (Fig. 6(f)), showing clearly identifiable structures such as side branches and micro vessels, which are washed out in the coarsely sampled commercial IV-OCT data set (Fig. 6(c)).

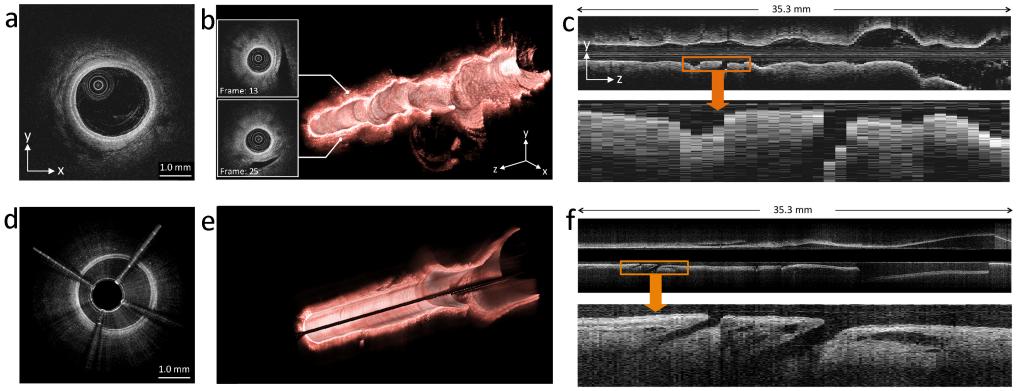

Fig. 6. Comparison of *in vivo* optical coherence tomography (OCT) images of the swine obtuse marginal (OM) branch. (a-c) Images acquired with a commercial OCT system, imaging at 100 frames/s and 20 mm/s pullback speed. (d-f) Images acquired with Heartbeat OCT at 3200 frames/s and 100 mm/s pullback speed. (a and d) Co-located cross-sectional images of a healthy artery (see Visualization 4) acquired with (a) commercial OCT and (d) Heartbeat OCT. (b and e) 3D reconstruction of the artery with (b) commercial OCT and (e) Heartbeat OCT. Due to the cardiac motion artifact, the same cross section appears twice in the images in (b). (c and f) Longitudinal rendering of the images (see Visualization 5) acquired with (c) commercial OCT and (f) Heartbeat OCT. The magnification shows the same region with two side branches.

3.3 In vivo imaging of coronary intervention and dissection

Following the imaging experiments in the native vessels, a bioresorbable vascular scaffold (3.0 x 18 mm, Abbott) was implanted in the mid-section of the LAD. The Heartbeat OCT catheter was accidentally inserted into a false lumen in between the scaffold struts and the adventitia (Fig. 7(a)), created by advancing the catheter into an artery with proximal acute angulation of the artery, partial proximal malposition and the lack of guidewire compatibility in this early prototype catheter. The intimal/medial flap in this dissection was visualized in great detail by the Heartbeat OCT system (Fig. 7(b) and 7(c)), allowing a faithful 3D reconstruction (Fig. 7(d)) and longitudinal rendering (Fig. 7(e)) of the vascular injury which was completely missed by angiography.

Imaging of the same structures with the commercial OCT system (Fig. 7(f)-7(h)), we can identify the same structures as observed with Heartbeat OCT. The cross-sectional images produced by the commercial system have slightly greater penetration depth due to better roll-off performance of the laser and obviously lack the shadows cast by the motor wires. We can see evidence of NURD, however, by the change in angular position of the dissection flap (Fig. 7(g) and 7(h)) and by the discontinuities in the longitudinal section (Fig. 7(f)), which also clearly shows the effect of undersampling.

#250211 Received 15 Sep 2015; revised 26 Oct 2015; accepted 30 Oct 2015; published 23 Nov 2015

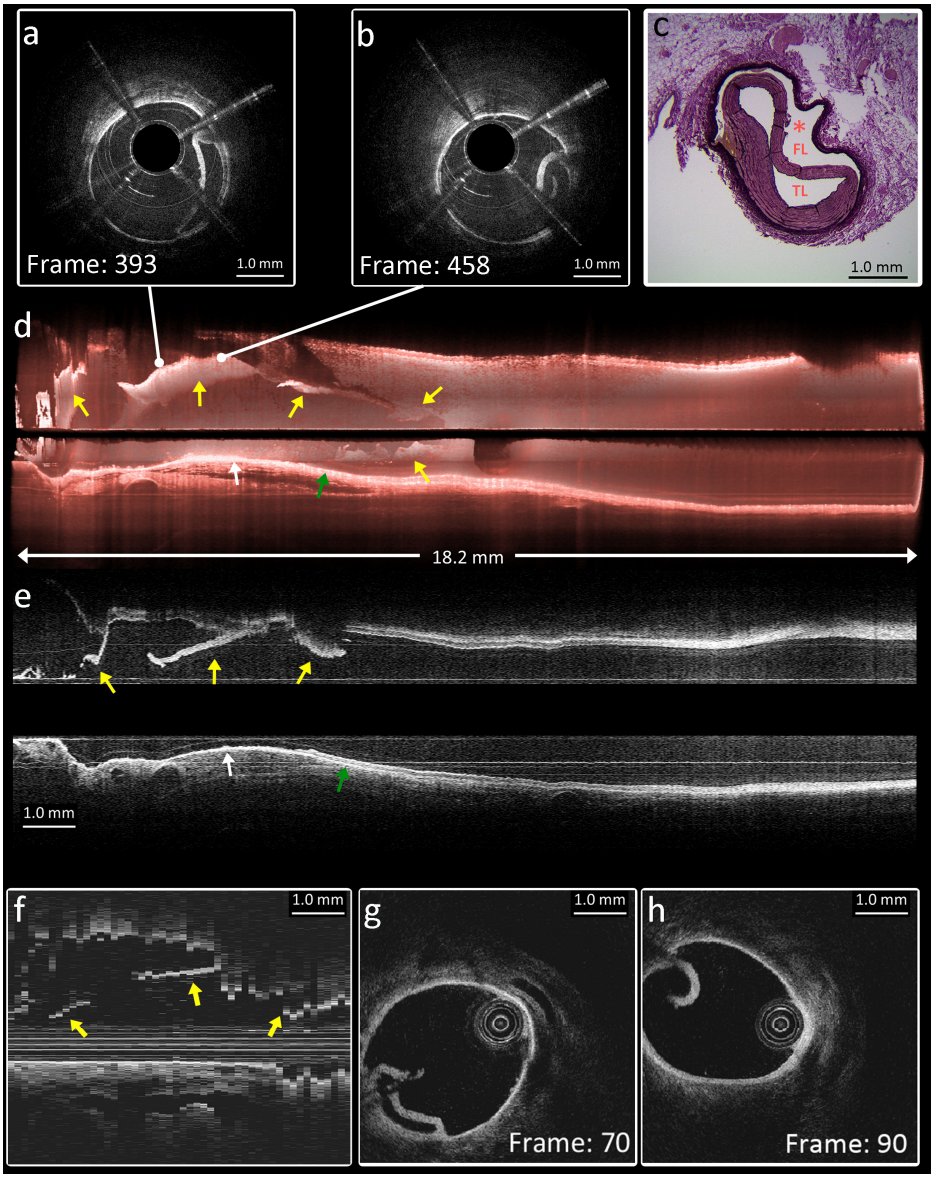

Fig. 7. *In vivo* images of intervention and dissection in LAD. Heartbeat OCT was imaging at 3200 frames/s and 100mm/s pullback speed. (a) and (b) Cross-sectional images of dissection. The OCT catheter (*) is located in the false lumen (FL) while the intima is stripped off the vessel circumference and compressed with an elliptic residual true lumen (TL) in 5 o'clock position. (c) Co-located histology of the dissection (resorcin fuchsine staining). (d) 3D reconstruction of 18.2 mm artery. (e) Longitudinal rendering of the images. In (d) and (e), the yellow arrows indicate the dissection flap. The white arrow indicates the exposed adventitia. The green arrow indicates a healthy artery wall with media and adventitia. (f-h) Comparison with the conventional OCT system: (f) Distal part of pullback, showing the same features as in (e) by yellow arrows, but undersampling and NURD affect continuity in this longitudinal section. (g) and (h) Cross-sectional images co-located with (a) and (b); showing the same features but with evidence of rotation due to NURD.

4. Discussion

Heartbeat OCT provides comprehensive imaging of the coronary vasculature *in vivo* at microscopic resolution, aimed at characterization of coronary artery disease and guidance of

#250211 Received 15 Sep 2015; revised 26 Oct 2015; accepted 30 Oct 2015; published 23 Nov 2015

coronary interventions. Capitalizing on the sweep speed of the FDML laser and the scan speed of the micro motor catheter, the scan rate of Heartbeat OCT (measured in samples per second) is greater than that of established technologies by a factor 20-30. This gain in acquisition speed is used to shorten the imaging time and to improve longitudinal image quality. The small frame spacing allows identification of microscopic tissue structures in the longitudinal views of the artery (see e.g. Figs. 6(f) and 7(e)). The resulting 3D reconstructions of the healthy swine vessels show smooth and tapered arteries, evidence of a faithfully rendered luminal geometry without cardiac motion during acquisition.

The distal motor employed for beam scanning overcomes artifacts related to non-uniform rotation. While previous methods for NURD correction, such as data registration [9, 27, 28] and signal mark methods [29, 30], have been moderately successful, the data acquired with the micromotor catheter achieves better fidelity with minimal post-processing. The small remaining angle error was corrected by aligning catheter features, as was demonstrated previously [18]. A marked difference with this earlier work is that the four wires together cast a shadow of less than 10% of the image.

Some motion correction in OCT pullbacks may be achieved in principle by coregistration with X-ray angiography, with which modern OCT systems achieve a high level of integration. However, the accuracy of the location information will be limited by the spatial (~300 μm) and temporal (30-40 ms) resolution of X-ray angiography. This is not sufficient to achieve the level of registration required to accurately position the OCT frames. Commercial coregistration is mainly targeting fused data visualization, and hence is not equipped for accurate OCT frame repositioning and reordering.

An additional potential advantage of the short imaging time is a reduction of the required flush volume, which may reduce the burden to the kidneys of the patient. Table 1 compares the parameters of Heartbeat OCT with other established endoscopic OCT systems [11, 13, 14, 31, 32].

Table 1. Comparison of endoscopic OCT speed

	Frame rate (frames/s)	A-line rate (kHz)	Pullback speed (mm/s)	Tip diameter mm	Sensitivity dB	Beam scanning
Heartbeat OCT	4000 *in vivo*	2.88×10^3	100	1.2	98	distal
Commercial [13, 33]	160-180 clinical	81-100	10 - 40	<0.9	not reported	proximal
Li et al. [31]	208 *in vitro*	50	N/A	1.65	111	distal
Tsai et al. [32]	400 *in vivo*	1×10^3	1	3.2	103	distal
Cho et al. [14]	350 *in vivo*	242.8	12	0.87	102.5	proximal

The micro motor catheter eliminates the need for a fiber-optic rotary junction. This configuration benefits advanced imaging techniques, e.g. combined OCT-fluorescence [34] or polarization-sensitive OCT [35], that offer new possibilities for tissue characterization. The large line density in the images will positively impact parametric OCT analyses that rely on high-quality data such as Doppler OCT [36], tissue type imaging [37], or elastography [38].

Further miniaturization of the motor, incorporation in a 1.0 mm outer sheath, and guidewire compatibility will be implemented in future designs. We will also minimize the impact of the wire shadows, which feature prominently in the images and may obscure relevant details such as dissections. One strategy to achieve this goal is by using thinner wires and mounting them on one side, aligned with the guidewire. However, the change in wire resistance and geometrical arrangement will require a new thermal evaluation. Use of a ball lens and a more flexible tube in the section between the fiber and the mirror will reduce the tip rigid length to 2-3 mm and thus improve tracking. With the current implementation of Heartbeat OCT, there is also room for a trade-off between pullback speed and pullback length, while still achieving an improvement in image quality of the longitudinal image

#250211 Received 15 Sep 2015; revised 26 Oct 2015; accepted 30 Oct 2015; published 23 Nov 2015

without cardiac motion artifacts. A future increase of the speed of the laser and micro motor may achieve even faster imaging that supports an even higher pullback speed.

FDML technology has been available for research purposes for several years now, and as the technology finds wider application, the cost of these lasers is set to become comparable to those used in present commercial systems. The entire system, including the laser, was integrated into a 100 x 50 x 60 cm movable cart, which still allows further integration. The catheter itself does not require any expensive parts. The micromotor replaces the flexible drive shaft common to today's catheters, and makes the IV-OCT system more robust because the rotary junction used in a conventional system is a failure-prone component that is subject to wear.

Regarding safety of the micromotor catheter, we do not foresee any issues with the current and voltage limited motor driver; the power of ~0.5 W is comparable to that delivered by modern IVUS catheters. Even if a catheter would mechanically fail, patients would not be exposed to hazardous levels of electrical energy. However, more pre-clinical experimental data need to definitively demonstrate safety, advantages and limitations of Heartbeat OCT.

5. Conclusions

We demonstrate Heartbeat OCT in full detail in this study. The system achieves an imaging speed of 4000 frames/s *in vivo*, which is 25 times higher than the commercial systems. Comparing with commercial systems, Heartbeat OCT provides faithful comprehensive *in vivo* OCT images by significantly depressing the cardiac motion artifacts, undersampling and NURD.

Acknowledgments

The authors acknowledge J. Meijer and B. Knapen from KINETRON B.V. for manufacturing the micro motor, C. Niles and R. van Duin for their contributions in the animal experiment preparation and histology preparation, R. Beurskens for building the power supply for the micro motor, and M. Gnanadesigan for contributions to image processing. This research was partly supported by the German Research Foundation (DFG-HU 1006/2, HU 1006/3, Cluster of Excellence: Munich Centre for Advanced Photonics) and the European Union (ERC, contract no.259158).

#250211 Received 15 Sep 2015; revised 26 Oct 2015; accepted 30 Oct 2015; published 23 Nov 2015